Received: 7 September 2023 | Revised: 1 December 2023 | Accepted: 14 December 2023

DOI: 10.1002/psp4.13102

ARTICLE

Maximum likelihood estimation of renal transporter ontogeny profiles for pediatric PBPK modeling

J. Porter Hunt[1] | **Samuel Dubinsky**[2] | **Autumn M. McKnite**[1] | **Kit Wun Kathy Cheung**[3] | **Bianca D. van Groen**[4] | **Kathleen M. Giacomini**[5] | **Saskia N. de Wildt**[6,7] | **Andrea N. Edginton**[2] | **Kevin M. Watt**[1]

[1]University of Utah, Salt Lake City, Utah, USA

[2]University of Waterloo, Waterloo, Ontario, Canada

[3]Genentech, Inc., South San Francisco, California, USA

[4]Roche Pharma and Early Development (pRED), Roche Innovation Center Basel, Basel, Switzerland

[5]UCSF, San Francisco, California, USA

[6]Erasmus MC, Rotterdam, The Netherlands

[7]Radboud University, Nijmegen, The Netherlands

Correspondence
Kevin M. Watt, 295 S. Chipeta Way, Salt Lake City, UT 84108, USA.
Email: kevin.watt@hsc.utah.edu

Abstract

Optimal treatment of infants with many renally cleared drugs must account for maturational differences in renal transporter (RT) activity. Pediatric physiologically-based pharmacokinetic (PBPK) models may incorporate RT activity, but this requires ontogeny profiles for RT activity in children, especially neonates, to predict drug disposition. Therefore, RT expression measurements from human kidney postmortem cortical tissue samples were normalized to represent a fraction of mature RT activity. Using these data, maximum likelihood estimated the distributions of RT activity across the pediatric age spectrum, including preterm and term neonates. PBPK models of four RT substrates (acyclovir, ciprofloxacin, furosemide, and meropenem) were evaluated with and without ontogeny profiles using average fold error (AFE), absolute average fold error (AAFE), and proportion of observations within the 5–95% prediction interval. Novel maximum likelihood profiles estimated ontogeny distributions for the following RT: OAT1, OAT3, OCT2, P-gp, URAT1, BCRP, MATE1, MRP2, MRP4, and MATE-2 K. Profiles for OAT3, P-gp, and MATE1 improved infant furosemide and neonate meropenem PBPK model AFE from 0.08 to 0.70 and 0.53 to 1.34 and model AAFE from 12.08 to 1.44 and 2.09 to 1.36, respectively, and improved the percent of data within the 5–95% prediction interval from 48% to 98% for neonatal ciprofloxacin simulations, respectively. Even after accounting for other critical population-specific maturational differences, novel RT ontogeny profiles substantially improved neonatal PBPK model performance, providing validated estimates of maturational differences in RT activity for optimal dosing in children.

Study Highlights

WHAT IS THE CURRENT KNOWLEDGE ON THE TOPIC?

Extrapolating adult physiologically-based pharmacokinetic (PBPK) models to pediatric populations requires a representation of renal transporter ontogeny.

However, this approach requires renal transporter ontogeny profiles that span the pediatric age spectrum.

WHAT QUESTION DID THIS STUDY ADDRESS?

Can renal transporter expression measurements provide reliable estimates of renal transporter ontogeny profiles for pediatric PBPK modeling?

WHAT DOES THIS STUDY ADD TO OUR KNOWLEDGE?

This study provides validated estimates of renal transporter ontogeny profiles that span the pediatric age spectrum. Profiles are estimated for the following 10 renal transporters: OAT1, OAT3, OCT2, P-gp, URAT1, BCRP, MATE1, MRP2, MRP4, and MATE-2K.

HOW MIGHT THIS CHANGE DRUG DISCOVERY, DEVELOPMENT, AND/OR THERAPEUTICS?

This work provides renal transporter ontogeny profiles for pediatric PBPK modeling for enhanced prediction of drug disposition in children and infants.

INTRODUCTION

Infants experience rapid developmental changes in physiological processes that directly affect drug pharmacokinetics (PKs) and thus optimal dosing.[1,2] As a result, optimal dosing predictions require a quantitative representation of the ontogeny, or maturational trajectory, of these processes. One of these processes is tubular secretion.[3,4] Tubular secretion is a major elimination pathway for many commonly used drugs and is driven primarily by renal transporters (RTs).[5,6] RT ontogeny has been evaluated primarily through mRNA and protein expression measurements in postmortem kidney samples.[4,7] These tissue measurements can be incorporated into physiologically-based PK (PBPK) models to improve predictions of the disposition of RT substrates in children.[8]

PBPK models can provide quantitative predictions of drug disposition in children by mechanistically representing relevant physiological processes from the population of interest.[9,10] PBPK models incorporating pediatric renal clearance have included the ontogeny of glomerular filtration and tubular secretion, and these approaches have demonstrated superior predictability compared with allometric scaling in children less than 2 years of age.[11–13]

Although these efforts have incorporated a measure of tubular secretion and RT ontogeny, transporter-specific ontogeny profiles that span the pediatric age spectrum to include preterm neonates are still needed.[14] Ideally, these profiles would provide estimates of the distributions of RT activity to facilitate pediatric population PBPK model predictions.

To provide such profiles, this work applies maximum likelihood estimation to RT expression measurements from human kidney postmortem cortical tissue samples to estimate ontogeny profiles for the following RT: OAT1, OAT3, OCT2, P-gp, URAT1, BCRP, MATE1, MRP2, MRP4, and MATE-2K. Profiles for OAT3, P-gp, and MATE1 are incorporated into pediatric population PBPK models for acyclovir, ciprofloxacin, furosemide, and meropenem – prevalent drugs for which limited data are available to guide optimal dosing.

METHODS

Renal transporter ontogeny data

The transporter expression measurements used in this work were previously measured from human postmortem renal cortical tissue samples obtained from biobanks in the United States and the Netherlands.[4] Both protein and mRNA expression measurements were made from human tissue samples and protein expression data were preferentially used to estimate ontogeny profiles. These protein and mRNA data were normalized by the mean mature expression level (Figure S1). Whereas the mean mature expression level would putatively be provided by the RT expression measurements from individuals older than 18 years (938 weeks) postmenstrual age (PMA; $n = 10$ per RT), we found no statistically significant difference (Welch's t-test; $p < 0.05$) in mean expression between individuals 5.5 years (288 weeks) to 18 years (938 weeks) PMA and individuals older than 18 years (938 weeks) PMA for any RT ($n = 13$ per RT; Figure S3). We therefore included expression measurements from all individuals older than 5.5 years (288 weeks) PMA ($n = 23$ per RT) to increase the sample size and more accurately estimate mature expression for each RT. Because RT expression data for the preterm neonate population consisted only of mRNA measurements, these measurements were normalized by

mature mRNA expression data in the same way protein expression data were normalized, and then combined with protein expression data. The extent to which protein and mRNA expression data were used to estimate the ontogeny profiles for each transporter is summarized in Table S1. To explore the impact of combining preterm neonate mRNA expression data, analogous ontogeny profiles were also estimated using only protein expression data (Table S1, Figure S5). Profiles that did not achieve mathematical convergence were estimated by manually and iteratively adjusting parameter values while assessing the visual fit and the value of the likelihood function (Table S1). For MRP2 and MRP4, no protein expression data were available; therefore, ontogeny profiles were estimated using only mRNA expression data. Neither protein nor mRNA expression preterm neonate data were available for URAT1 and BCRP. Therefore, URAT1 and BCRP profiles were estimated using only protein data. Consequently, except for URAT1 and BCRP, ontogeny data represent the pediatric age spectrum from 25 weeks PMA to older than 30 years of age. More than 62 expression measurements, including more than 32 measurements from individuals less than 2 years of age, informed the estimation of every ontogeny profile (Table S1).

Maximum likelihood estimation of renal transporter ontogeny profiles

Preliminary nonlinear least squares regression of RT expression data was challenging, likely because of the heteroscedasticity of the data. Therefore, this work used maximum likelihood estimation to fit a heteroscedastic sigmoidal mathematical equation as a function of PMA to the RT expression data. Four sigmoidal equations were investigated (Figure S2): Gompertz (Equation S3); Logistic (Equation S4); Weibull (Equation S5); and Hill (Equation 1). The Hill equation[15] was chosen for all ontogeny profiles because it resulted in the highest overall likelihood when fit to the median of the normalized RT expression data. RT expression data were fit with a lognormal distribution because this distribution is most appropriate for processes that result from multiplicative interactions, including transporter kinetics.[16] Whereas normally distributed ontogeny profiles were also estimated (Equation S1; Figure S4), lognormally distributed profiles demonstrated greater mathematical convergence (Table S1). The maximum likelihood estimation resulted in heteroscedastic, lognormally distributed ontogeny profiles for pediatric PBPK modeling.

$$f_i(x_i, a, b) = \left[1 + \left(\frac{a}{x_i}\right)^b\right]^{-1} \quad (1)$$

In Equation 1, a and b are function parameters and x is the PMA in years. Within the maximum likelihood estimation, this function informed the likelihood function (Equation 2), which calculates the likelihood of observing the data given the parameter values of the function. The likelihood function also included an estimate of the variance (σ_i) of the ontogeny as a function of PMA (Equations 3 and S2) so that a distribution for each age could be simultaneously estimated. The best estimates of these parameters were then determined by maximizing the likelihood of observing the normalized expression data.[17] The optimal ontogeny profiles and distributions with lognormally distributed variance were estimated by maximizing the likelihood function (Equation 2):

$$L(\mathbf{Y}|\,\mathbf{X}, a, b, s) = \prod_{i=1}^{n} \frac{1}{y_i \sigma_i \sqrt{2\pi}} \exp\left\{ \frac{-\left[\ln\left(\frac{y_i}{f_i}\right)\right]^2}{2{\sigma_i}^2} \right\} \quad (2)$$

$$\sigma_i(x_i, a, b, s) = s \bullet \exp(-f_i) \quad (3)$$

In these mathematical expressions, f represents Equation 1 and is the median of the ontogeny distributions for lognormally distributed ontogeny profiles; and s is the proportionality constant that relates the value of the median or mean (for lognormally or normally distributed profiles, respectively) of the ontogeny distribution for a given age with its variance (Equation 3). The data permitted mathematical convergence for seven and five out of 10 transporters for lognormally and normally distributed ontogeny profiles, respectively (Table S1). The maximum likelihood values of a, b, and s for each ontogeny distribution are given in Table S1. Tables of the resulting ontogeny distributions for incorporation into PBPK models are included as Tables S2–S11.

Pediatric PBPK modeling using maximum likelihood ontogeny profiles

PBPK modeling was accomplished with PK-Sim version 11 from the Open Systems Pharmacology suite. PK-Sim was programmed as described below with maximum likelihood ontogeny profiles. From these ontogeny profiles, a dimensionless ontogeny scaling factor (OSF) as a function of PMA is used to calculate the effective RT concentration for each virtual pediatric individual according to Equation 4.

$$[\mathrm{RT}]_{\mathrm{ped}}(\mathrm{PMA}) = [\mathrm{RT}]_{\mathrm{adult}} \bullet \mathrm{OSF}(\mathrm{PMA}) \quad (4)$$

In Equation 4, $[RT]_{ped}$ is the kidney RT concentration of the virtual pediatric individual. The adult renal transporter concentration ($[RT]_{adult}$) was derived from literature or identified in the adult model (Figure 1a; Table S12). For individual simulations, the OSF is determined by the lognormally distributed maximum likelihood ontogeny profile as the median of the ontogeny distribution for that individual's age. For population simulations, the PK-Sim algorithm for creating virtual populations assigns OSFs to virtual individuals by sampling from the age-appropriate distribution of the ontogeny profile. Thus, for population PBPK simulations, the OSF is a lognormally distributed variable.

The drug's molar rate of mass transport for both the basolateral (kidney interstitial to kidney intracellular) and apical (kidney intracellular to urine) active transport processes were simulated with Michaelis–Menten kinetics. The K_m and k_{cat} parameter values were derived from literature reports of in vitro experiments or identified in the adult simulations (Figure 1a, Table S12), including with adult probenecid simulations described in the subsequent section. Although these validated parameter values are utilized directly in pediatric PBPK models, simulated renal active transport of the drug is also determined by the appropriate RT ontogeny function, as described by Equation 5:

$$\text{Active transport rate}\left(\frac{\text{mol}}{\text{time}}\right) = [RT]_{ped} \bullet V_{kid} \bullet k_{cat} \bullet \frac{[D]}{K_m + [D]} \quad (5)$$

In Equation 5, $[RT]_{ped}$ is the molar concentration of renal transporter in the kidneys described by Equation 4, $[D]$ is the molar concentration of drug in the interstitial (basolateral transport) or intracellular (apical transport) compartment, V_{kid} is the kidney volume scaled according to the age of the simulated individual,[18] k_{cat} is the Michaelis–Menten transporter turnover number, and K_m is the transporter Michaelis–Menten constant. The PBPK model attributes basolateral and apical transporters to the kidney interstitial and kidney intracellular compartments of the model, respectively.

Ontogeny profile and PBPK model validation

For the validation of ontogeny profiles, PBPK models were first constructed without RT ontogeny profiles. Then, RT ontogeny profiles were incorporated and the improvement in model performance was assessed. PBPK models were constructed with established methods[19,20] that were adapted in the following ways (Figure 1a): (1) adult model kidney parameters describing basolateral and apical processes were estimated using PK data from drug–drug interaction (DDI) studies with probenecid in order to more accurately estimate the relative contribution of each transport process to overall tubular secretion;[21,22] (2) the ontogeny of tubular secretion was represented using the OAT3, P-gp, and MATE1 ontogeny profiles of this work and applied to drug-specific models as directed by a literature review of drug-transporter interactions.[5]

The development of adult acyclovir, ciprofloxacin, furosemide, meropenem, and probenecid PBPK models has

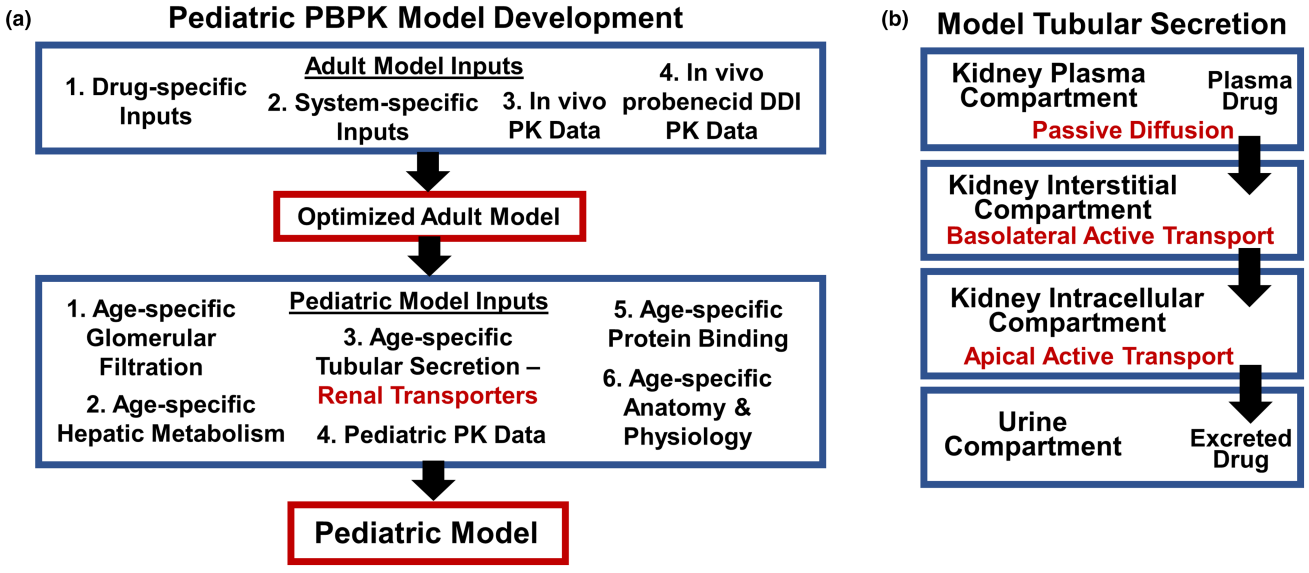

FIGURE 1 (a) Workflow of pediatric renal transporter PBPK model development. Drug-specific inputs include physicochemical properties. System-specific inputs include population-specific organ weights and blood flows. (b) Diagram of PK-Sim PBPK kidney compartments (plasma, interstitial, intracellular, and urine) and processes comprising modeled tubular secretion. DDI, drug–drug interaction; PBPK, physiologically-based pharmacokinetic; PK, pharmacokinetic.

been previously reported,[21,22] with parameter identification repeated for PK-Sim version 11. As a critical step in the process for creating reliable pediatric PBPK models, the performance of these adult models was rigorously validated. Optimal adult parameter values are presented in Table S12.[23–29]

Pediatric PBPK model development begins with the optimized adult model and comprises the following steps: (1) drug-specific model inputs (e.g., physicochemical properties, k_{cat} and K_m parameter values for enzymatic and transport processes) are kept constant; (2) physiological measures specific to pediatric populations, including organ volumes and blood flow rates are changed from adult values to age-specific pediatric values using PK-Sim and as reported in literature[9,18]; and (3) OSFs are used to calculate parameter values for maturation-dependent processes.[18] These maturation-dependent processes include the following: (1) glomerular filtration; (2) the maturation-dependent activity of hepatic metabolizing enzymes (e.g., UGT1A9); (3) albumin ontogeny and its effect on protein binding; and (4) the age-dependent tissue expression of transporters (e.g., OAT3 and MRP4).[18] PK-Sim incorporates maturation functions for (1) through (3), including heteroscedastic, lognormally distributed ontogeny profiles for the major metabolizing enzymes across the pediatric age spectrum. In contrast, ontogeny profiles required by (4) are not available.

For each pediatric population PBPK simulation, 1000 virtual pediatric individuals were created to reflect the patient demographics within each respective study. Variability was assigned to each clearance process and integrated within the population PBPK simulations (Table S13). The ability of each model to accurately represent the PK of each drug of interest at the population level was assessed with the mean or median as specified and with the 5th to 95th percentile prediction interval of drug concentrations for the population. Model performance was evaluated using the percentage of individual drug concentrations falling within the 5th to 95th percentile prediction interval, average fold error (AFE; Equation 6), and absolute average fold error (AAFE; Equation 7) with respect to plasma concentrations.

$$\mathrm{AFE} = 10^{\frac{1}{N}\sum_i \log\left(\frac{\mathrm{predicted}_i}{\mathrm{observed}_i}\right)} \tag{6}$$

$$\mathrm{AAFE} = 10^{\frac{1}{N}\sum_i \left|\log\left(\frac{\mathrm{predicted}_i}{\mathrm{observed}_i}\right)\right|} \tag{7}$$

In Equations 6 and 7, $\mathrm{predicted}_i$ and $\mathrm{observed}_i$ correspond to predicted and observed plasma concentrations, respectively. AFE and AAFE assessed model bias and precision, respectively, for individual measurements and cohort averages (furosemide and meropenem),[30] whereas percentage within the 5th to 95th percentile assessed model performance with aggregated data points from literature (ciprofloxacin and acyclovir).[31,32] Acceptable model performance required AFE of 0.7 to 1.3 and AAFE less than or equal to two or 80–95% of observed individual drug concentrations within the 5th to 95th percentile prediction interval.

Pediatric PBPK models for acyclovir, ciprofloxacin, furosemide, and meropenem

Acyclovir clearance is represented by the following processes: (1) renal clearance through glomerular filtration; (2) renal clearance through tubular secretion mediated by OAT3 and an apical transporter process (representing MATE and BCRP)[5]; and (3) generic hepatic metabolism by an unknown enzyme modeled as first order degradation. The maximum likelihood ontogeny profiles for OAT3 and MATE1 were applied to the basolateral and apical active transport processes, respectively. The performance of the pediatric PBPK model for acyclovir was assessed using literature PK data[33] as the proportion of observations captured within the 5th to 95th percentile prediction interval of population PBPK simulation results[31,32] (Figure 3b).

Ciprofloxacin clearance is represented by the following processes: (1) renal clearance through glomerular filtration; (2) renal clearance through tubular secretion mediated by OAT3 and an apical transport process (Table S12)[5]; and (3) hepatic metabolism by CYP1A2 modeled as first order degradation. Ontogeny for CYP1A2 was represented by the PK-Sim ontogeny profile for CYP1A2. Ontogeny for OAT3 was represented by the OAT3 maximum likelihood ontogeny profile. Although the contribution of specific RTs to apical efflux of ciprofloxacin is unclear,[22] the maximum likelihood ontogeny profile for MATE1 was applied to the apical active transport process because (1) ciprofloxacin is a known substrate of MATE1[34]; (2) ciprofloxacin perpetrates transport inhibition of other MATE1 substrates[35]; and (3) the role of BCRP and P-gp in apical efflux of ciprofloxacin is contested.[5,36,37] The performance of the pediatric PBPK model for ciprofloxacin was assessed using literature PK data[38,39] as the proportion of observations captured within the 5th to 95th percentile prediction interval of population PBPK simulation results.[31,32]

Furosemide clearance is represented by the follow processes: (1) renal clearance through glomerular filtration; (2) renal clearance through tubular secretion mediated by OAT3 and a combination of MRP2, MRP4, and P-gp[21]; and (3) metabolism through glucuronidation by UGT1A9 with expression following the PK-Sim gene expression database. Ontogeny for UGT1A9 was represented by the PK-Sim ontogeny profile for UGT1A9 (Figure S6). The

ontogeny profile for OAT3 from this work was applied to the basolateral OAT3 transport process. Literature evidence is conflicting regarding furosemide as a substrate of MRP2 and P-gp.[36,40–42] Additionally, the P-gp ontogeny profile achieved mathematical convergence whereas the ontogeny profiles for MRP2 and MRP4 did not. Therefore, the P-gp ontogeny profile from this work was applied to the apical transport process. The performance of the pediatric PBPK model for furosemide in the preterm neonate and infant populations was assessed using AFE and AAFE[31,32] and the proportion of observations captured within the 5th to 95th percentile prediction interval of population PBPK simulation results using literature PK data.[43,44]

Meropenem clearance is represented by the follow processes: (1) renal clearance through glomerular filtration; (2) renal clearance through tubular secretion mediated by OAT3 and a generic apical transporter process; (3) metabolic clearance by dehydropeptidase (DHP). The DHP activity was assumed to be mature in all patient populations simulated as no ontogeny data could be found for DHP in the literature. The ontogeny profile for OAT3 from this work was applied to the basolateral OAT3 transport process.[45] Because the apical transport of meropenem is not known, and a recent report suggests that meropenem is not a substrate of any apical transporter studied in this work,[46] the ontogeny profile for OAT3 was also applied as a surrogate for maturation of the apical transport process. The performance of the pediatric PBPK model for meropenem was assessed using AFE and AAFE from literature PK data.[47,48]

PK-Sim model files for each drug are included with the Supplementary Material.

Sensitivity analysis

A local sensitivity analysis was performed to investigate the influence of RT ontogeny within the pediatric PBPK simulations on primary PK parameters such as the area under the curve extrapolated to infinity (AUC_{∞}) and total clearance (CL_{total}). Specific RT activity involved in the clearance pathways of each drug was varied by 10% and the relative changes in AUC_{∞} and CL_{total} were reported as sensitivity coefficients. RT concentration incorporated within each model was used as a surrogate for testing the importance of the newly developed OSF on each PK parameter of interest. The sensitivity coefficient (S^p) for the effect of the parameter (p) on the PK output (PK) was calculated as the average of Equation 8:

$$S^p = \left| \frac{PK(p + 0.1 \times p) - PK(p)}{PK(p)} \right| \times \frac{100\,\%}{10\,\%} \qquad (8)$$

A sensitivity coefficient of 1 means that a 10% change in the parameter value caused a ±10% change in the PK output, and a sensitivity coefficient of 0.1 means that a 10% change in the parameter value caused a ±1% change in the PK output.

RESULTS

Heteroscedastic ontogeny profiles were estimated for the following RT: OAT1, OAT3, OCT2, P-gp, URAT1, BCRP, MATE1, MRP2, MRP4, and MATE-2 K (Figure 2a). Alternative ontogeny profiles were estimated using only protein expression data by excluding mRNA expression measurements from preterm neonates. Two outliers were excluded before the estimation of the P-gp and URAT1 ontogeny profiles.[49] The ontogeny profiles are defined by Equations 1–3, with function parameters given in Table S1. These profiles, including variance as a function of PMA, are tabulated as Tables S2–S11.

The ontogeny profile for P-gp is shown in Figure 2b together with observed data and virtual population OSF results from PK-Sim. The observed data are shown in red, whereas the simulated OSFs are shown in gray. For comparison, an ontogeny profile for generic active tubular secretion of PAH previously reported by Hayton[50] is included in Figure 2a.

The performance of the maximum likelihood ontogeny profiles for OAT3, P-gp, and MATE1 was assessed with pediatric population PBPK simulations of acyclovir, ciprofloxacin, furosemide, and meropenem. These results demonstrate significantly improved model performance for preterm neonate and neonate populations after incorporating ontogeny profiles. Literature PK data are summarized in Table 1 and PBPK model performance with and without ontogeny profiles is summarized in Table 2. Table S14 summarizes pediatric PBPK model performance after incorporating ontogeny profiles estimated from only protein expression data (i.e., that omit preterm neonate mRNA expression data).

Literature acyclovir data included 50 pediatric patients ages newborn to 18 years[33] and simulation results are shown in Figure 3b. Sevent-three percent and 74% of observed concentrations were captured within the 5th to 95th percentile prediction interval for simulations with and without ontogeny profiles, respectively.

Ciprofloxacin data from the literature included 60 neonates and preterm neonates,[39] 10 infants ages 3–12 months,[38] and 10 children ages 12–60 months.[38] For the neonatal population simulation, ontogeny profiles improved model AFE from 0.17 to 0.62, AAFE from 6.10 to 1.96, and the proportion of data falling within the 5th to 95th percentile prediction interval from 48% to 98%

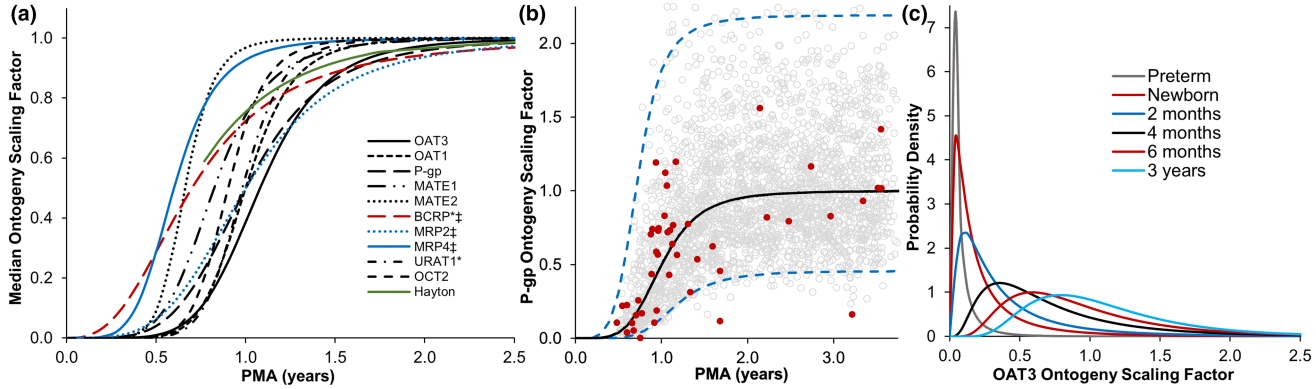

FIGURE 2 (a) Lognormally distributed ontogeny profiles for individual renal transporters resulting from renal cortical tissue expression measurements and maximum likelihood estimation. (b) Lognormally distributed P-gp ontogeny profile. Red dots represent normalized observed expression levels; the black line is the maximum likelihood fit of the sigmoidal Hill equation to the median of the distributions. Dotted lines represent two standard deviations from the median. Gray dots represent P-gp OSF produced by a population PBPK simulation in PK-Sim. (c) Probability density functions of the estimated population distributions of OAT3 OSF at six different pediatric ages: preterm (PMA = 31 weeks), newborn (PMA = 42 weeks), 2 months (PMA = 47 weeks), 4 months (PMA = 57 weeks), 6 months (PMA = 63 weeks), and 3 years (PMA = 198 weeks). ‡Profiles estimated by manual, iterative parameter adjustments rather than by mathematical convergence. *No preterm neonate expression data available for these transporters. OSF, ontogeny scaling factor; PBPK, physiologically-based pharmacokinetic; PMA, postmenstrual age.

TABLE 1 Pediatric pharmacokinetic data for acyclovir, ciprofloxacin, furosemide, and meropenem.

Drug	Study	# Patients	Age	Dose
Acyclovir	Abdalla et al.	50	0.02 to 18 years	17 mg/kg i.v.[a]
Ciprofloxacin	Zhao et al.	60	25–48 weeks PMA	9.7 mg/kg i.v.[a]
	Lipman et al.	10	3–12 months	10 mg/kg i.v.
		9	12–60 months	10 mg/kg i.v.
Furosemide	Peterson et al.	1	18-day-old preterm neonate	1 mg/kg i.v.
		1	3-month-old infant	1 mg/kg i.v.
		1	4-month-old infant	1 mg/kg i.v.
	Tuck et al.	1	38-week PMA preterm neonate	1 mg/kg i.v.
Meropenem	van den Anker et al.	23	Preterm neonates	10 mg/kg i.v. 20 mg/kg i.v. 40 mg/kg i.v.
		15	Term neonates	10 mg/kg i.v. 20 mg/kg i.v. 40 mg/kg i.v.
	Blumer et al.	63	2-months to 12 years	10 mg/kg i.v. 20 mg/kg i.v. 40 mg/kg i.v.

Abbreviation: PMA, postmenstrual age.

[a]Cohort median dose.

(Figure 3a). Simulation results for the pediatric ciprofloxacin cohorts are included as Figure S8.

PK data for furosemide from the literature included two preterm neonates and two infants (Figure 4). Comparing the population PBPK simulation median peripheral venous plasma furosemide concentration with observed literature data, the combined AFE and AAFE for all four patients improved from 0.08 to 0.70 and 12.08 to 1.44, respectively, after the incorporation of ontogeny profiles. Notably, 0% of preterm neonate observed data fell within the 5th to 95th percentile prediction interval without the incorporation of ontogeny profiles compared with 85% of the preterm neonate data with ontogeny profiles (Table 2).

TABLE 2 Pediatric PBPK model performance for acyclovir, ciprofloxacin, furosemide, and meropenem before and after incorporating renal transporter ontogeny.

	No RT ontogeny			With RT ontogeny		
Drug	**AFE**	**AAFE**	**In 5–95%**	**AFE**	**AAFE**	**In 5–95%**
Acyclovir						
0.02–18 years PNA ($n=50$)	0.766	2.304	73%	0.755	2.306	74%
Ciprofloxacin						
25–48 weeks PMA ($n=60$)	0.169	6.102	48%	0.620	1.961	98%
3–60 months PNA ($n=19$)	1.098	1.200	NA[a]	1.201	1.235	NA[a]
Furosemide						
Preterm neonates ($n=2$)	0.030	33.267	0%	0.722	1.386	85%
3–4 months PNA ($n=2$)	0.358	2.793	33%	0.671	1.520	89%
Infant total ($n=4$)	0.083	12.075	14%	0.700	1.439	86%
Meropenem						
Neonates ($n=38$)	0.531	2.093	NA[a]	1.336	1.358	NA[a]
2–144 months PNA ($n=63$)	0.752	1.541	NA[a]	0.747	1.543	NA[a]

Abbreviations: AFE, average fold error; AAFE, absolute average fold error; NA, not available; PBPK, physiologically-based pharmacokinetic; PMA, post-menstrual age; PNA, post-natal age; RT, renal transporter.

[a]Data from individual study participants not available.

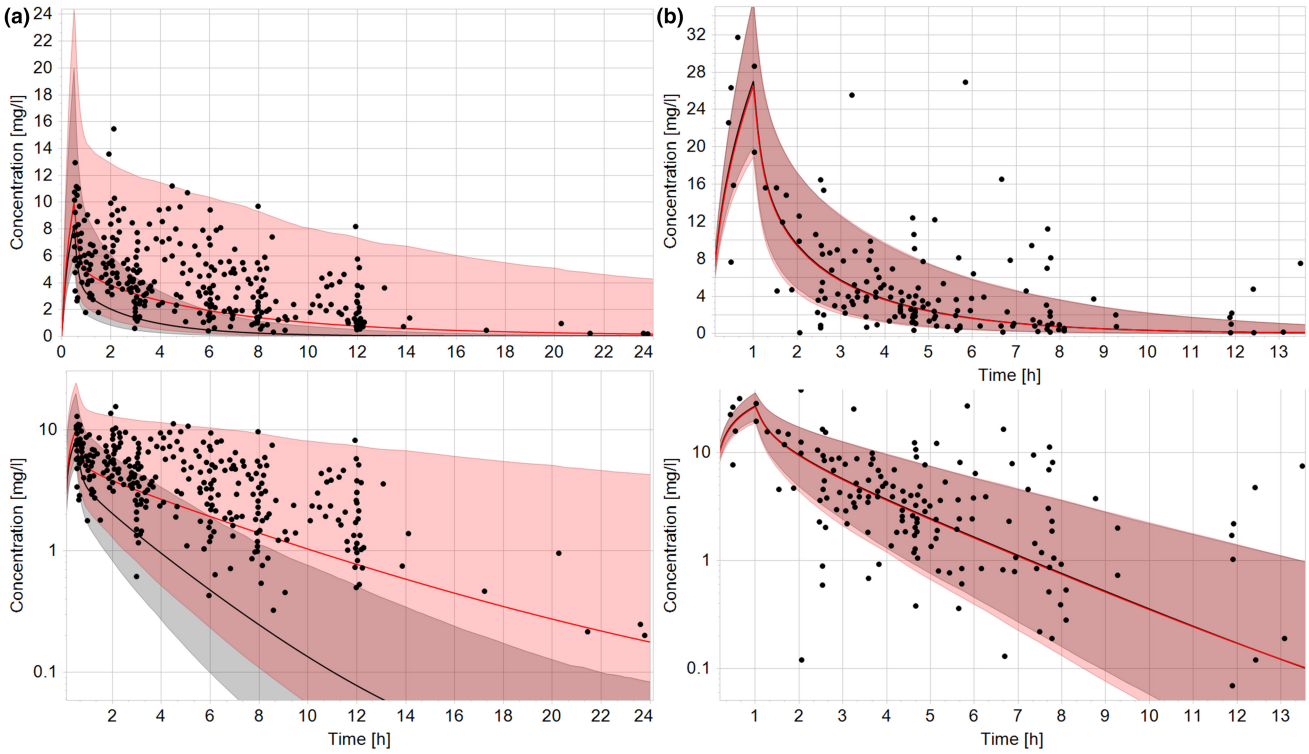

FIGURE 3 Pediatric population PBPK simulations of (a) ciprofloxacin (Zhao et al.,[39] $n=60$ neonates ages 25–41 weeks PMA) and (b) acyclovir (Abdalla et al.,[33] $n=50$ pediatric patients ages newborn to 18 years). Black and red lines represent virtual population medians without and with renal transporter ontogeny, respectively. Shaded regions represent corresponding 5th to 95th percentile simulated concentration ranges. The PBPK population comprised 1000 virtual individuals with characteristics corresponding to the literature cohorts. PBPK, physiologically-based pharmacokinetic; PMA, postmenstrual age.

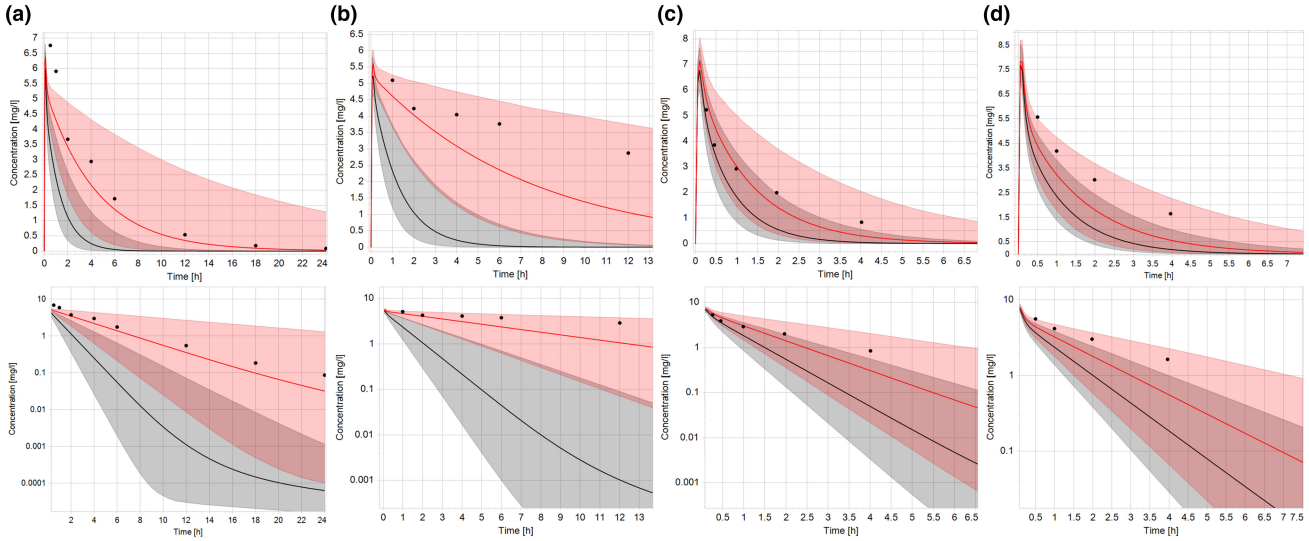

FIGURE 4 Pediatric population PBPK simulations and observed data of furosemide after administration of 1 mg/kg by i.v. infusion. (a) Preterm neonate[44]; (b) Preterm neonate[43]; (c) 3-month-old infant[43]; and (d) 4-month-old infant.[43] Black and red lines represent virtual population medians for simulations without and with renal transporter ontogeny, respectively. Shaded regions represent corresponding 5th to 95th percentile simulated concentration ranges. The PBPK populations comprised 1000 virtual individuals with characteristics corresponding to the literature cohorts. PBPK, physiologically-based pharmacokinetic.

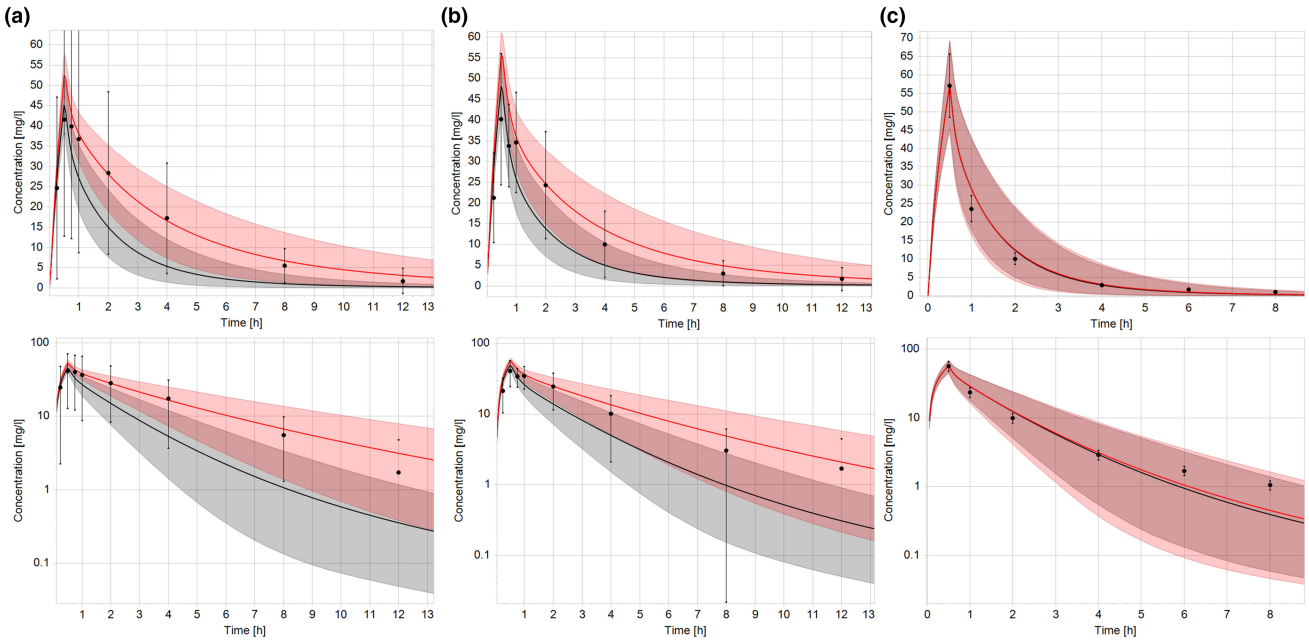

FIGURE 5 Pediatric plasma PK data and population PBPK simulation results after 20 mg/kg meropenem i.v. over 30 min. (a) Preterm neonates ($n = 8$)[47]; (b) full-term neonates ($n = 5$)[47]; and (c) pediatric cohort ages 2 months to 12 years ($n = 25$).[48] Black and red lines represent virtual population arithmetic means for simulations without and with renal transporter ontogeny, respectively. Shaded regions represent corresponding 5th to 95th percentile simulated concentration ranges. The PBPK populations comprised 1000 virtual individuals with characteristics corresponding to the literature cohorts. Additional meropenem simulation results are included as Figure S11. PBPK, physiologically-based pharmacokinetic; PK, pharmacokinetic.

PK data for meropenem included plasma concentrations from 23 preterm neonates,[47] 15 full-term neonates,[47] and 63 infants and children aged 2 months to 12 years.[48] Plasma meropenem PK data and simulation results are shown in Figures 5, S10, and S11. Comparing population PBPK arithmetic means to PK study cohort averages, the combined AFE and AAFE for all six preterm and term neonate population simulations improved from 0.54 to 1.34 and 2.09 to 1.36, respectively, after incorporating ontogeny profiles.

The PK parameters for all four drugs demonstrate notable sensitivity to changes in RT concentration (Figure S12).

DISCUSSION

Because RTs contribute significantly to the disposition of many drugs, an accurate representation of their ontogeny is critical to predict exposure to these drugs in infant populations, especially when extrapolation of an adult PBPK model is necessary. This is demonstrated by the significant difference in neonate PBPK model performance between models which incorporate RT ontogeny and models that do not. These differences remain significant notwithstanding the incorporation of other critical population-specific maturational differences such as glomerular filtration (Figure 1). Notably, if dosing of these drugs were guided by neonate PBPK simulations without RT ontogeny, overexposure is the expected result.

The ontogenies for all RT estimated in this work achieve mature levels by 2 years PMA. Interestingly, the RTs studied in this work follow more rapid maturational trajectories than many metabolizing enzymes.[51] Concordantly, PBPK simulations of older pediatric cohorts show less improvement in performance after incorporating ontogeny profiles compared with the dramatic improvements in simulations of neonates and preterm neonates after incorporating ontogeny profiles (Table 2). For example, simulations of furosemide in 3 and 4-month-old infants show significantly less negative deviation from observed data when ontogeny is omitted than the simulations for preterm neonates (Figure 4).[43] Similarly, the accurate and similar performance of acyclovir simulations with and without ontogeny may be attributed to the wide age range of study participants (0.02–18 years).[33] Importantly, the available literature PK data do not allow a direct assessment of the maximum likelihood ontogeny profiles within the acyclovir pediatric PBPK model for children less than 2 years of age. However, these results do demonstrate that ontogeny profiles perform well for this combined cohort of older children plus neonates. Likewise, simulations of neonate and preterm neonate meropenem cohorts are dramatically less biased by including the OAT3 ontogeny profile, whereas no changes are observed in the simulation of the cohort with a mean of 4 years old (Figures 3 and 5).[47,48] Furthermore, simulations of the ciprofloxacin cohort consisting of children between 3 and 12 months old (1–1.7 years PMA) without ontogeny show only moderate deviations from observed data (Figure S8), whereas simulations without ontogeny of neonates receiving ciprofloxacin show significant deviation from observed data (Figure 3).[38] This suggests that these ontogeny profiles represent the maturation of RT activity in these patient cohorts.

The local sensitivity analyses are likewise instructive. As highlighted by the sensitivity analysis for meropenem, the OSF of OAT3 became slightly less influential on the PK parameters with increasing age, which is demonstrated by the decreasing sensitivity between simulations of preterm neonates and older children. This is likely a result of the model correctly representing the maturation of pediatric GFR: as GFR increases, the contribution of RT to overall clearance decreases. The results of these analyses convey the importance of maturational functions in the context of PBPK modeling, and their ability to accurately describe the PK of renal transporter substrates across the age spectrum.

An important feature of the profiles reported in this work is their heteroscedasticity, which estimates the variance of RT activity across the pediatric age spectrum based on observed expression data. Such estimates enable more accurate population PBPK predictions. Although both normally and lognormally distributed ontogeny profiles were estimated, lognormally distributed ontogeny profiles provided superior estimates of the renal transporters studied in this work and may be preferred in PBPK modeling based on the apparent distributions of the available RT expression data in adults. Measurements of OAT3 expression in mature populations have resulted in coefficient of variation (CV) of 0.44 and 0.48.[52,53] By comparison, sampling from the mature distribution of the OAT3 ontogeny profile (Figure 2b) resulted in a CV of 0.50. Thus, population PBPK model simulations utilizing these profiles represent appropriate variability.

This PBPK modeling approach provides a tool to understand and predict RT mediated DDIs in pediatric populations.[21] By leveraging probenecid DDI PK data,[22] the method used in this work represents the apical and basolateral transport rates separately. Although this method also requires separate apical and basolateral ontogeny profiles, it retains distinct advantages, such as the potential to capture a flux imbalance and subsequent intracellular accumulation across the tubule epithelium. High tubule intracellular concentrations have been implicated in the renal toxicity of several drugs,[54,55] and this mechanistic PBPK approach may help identify such mechanisms of renal toxicity. For example, if the relevant basolateral transport process matures more rapidly than the apical transport process, infants may be susceptible to renal toxicities to which patients with mature RT activities are not. Importantly, the local sensitivity analyses demonstrate that renal transporter ontogeny significantly influences the simulated PKs of these drugs.

This work is not without limitations. First, this approach assumes that tissue-specific transporter

expression represents transporter activity. If RT expression is not analogous to RT activity in the tubules, additional considerations may be required to predict pediatric PKs. However, the good performance of the pediatric models suggests that these ontogeny profiles provide useful estimates of RT activity. Additionally, our data suggest that URAT1 expression may peak around 3 years PMA before decreasing to adult levels. Although this nonmonotonic profile may not be fully captured by the monotonic ontogeny functions used in this work, URAT1 is the only RT for which our data suggest a nonmonotonic maturational trajectory, and the estimation of a nonmonotonic ontogeny function is left to future work. Additionally, mRNA data from preterm neonates were normalized to mature levels and then combined with protein expression data to ensure that the preterm neonate population was represented in the final ontogeny profiles. To investigate the appropriateness of combining protein and mRNA expression data, ontogeny profiles were also created after excluding preterm neonate mRNA expression data. Overall, these profiles did not perform as well in PBPK models compared to the profiles that included mRNA expression data (Table 2, Table S14). Nevertheless, because preterm neonate mRNA expression data were not available for URAT1 and BCRP, these ontogeny profiles may not be fully representative of this population. Importantly, the ontogeny profiles that were estimated with preterm neonate data and converged to a mathematical solution (Figure 2a, Table S1), are likely most representative of the RT ontogeny of these populations. Specifically, lognormally distributed profiles for BCRP, MRP2, and MRP4 were estimated without mathematical convergence (Figure 2a, Table S1) and therefore population representativity is less likely. Additional data for these transporters may facilitate more reliable estimates of ontogeny distributions. Notwithstanding, all other lognormally distributed ontogeny profiles converged to mathematical solutions, and the ontogeny profiles for MATE1, OAT3, and P-gp significantly improved infant PBPK model performance, suggesting that these profiles are representative of RT ontogeny in these populations. The estimation method provided by this work could be applied to other ontogenies, (e.g., organ volumes, binding partners, and metabolizing enzymes) to further improve pediatric PBPK modeling.

In conclusion, this study addresses a major gap in drug dosing and development by providing estimates of heteroscedastic RT ontogeny profiles to facilitate pediatric PBPK modeling of RT substrates across the pediatric age spectrum. The value of this contribution is highlighted by recommendations from regulatory authorities to utilize in silico methods, such as PBPK models that incorporate drug metabolizing enzymes and drug transporters to inform clinical studies of drugs in pediatric patients of all ages. Whereas accurate PK predictions can be especially difficult in preterm and term neonate populations, these simulations provide reasonable predictions enabled by novel RT ontogeny profiles in these vulnerable populations.

AUTHOR CONTRIBUTIONS

All authors wrote the manuscript. J.P.H., S.D., A.N.E., and K.M.W. designed the research. J.P.H., S.D., A.N.E., K.M.W., K.W.K.C., B.D.vG., K.M.G., and S.N.dW. performed the research. J.P.H., S.D., A.N.E., and K.M.W. analyzed the data.

ACKNOWLEDGMENTS

The authors thank Professor Larry Baxter of Brigham Young University for exceptional statistics instruction, Michael Sevestre and the Open Systems Pharmacology community for PK-Sim software support, and the Division of Clinical Pharmacology at the University of Utah for insightful discussions.

FUNDING INFORMATION

J.P.H. receives support from the Thrasher Research Fund. A.M.M. receives support from the National Institute of Diabetes and Digestive and Kidney Diseases (F31DK130542). K.M.W. receives research support from the National Institute of Child Health and Human Development (R01HD097775 and R21HD104412).

CONFLICT OF INTEREST STATEMENT

The authors declared no competing interests for this work.

REFERENCES

1. Kearns GL, Abdel-Rahman SM, Alander SW, Blowey DL, Leeder JS, Kauffman RE. Developmental pharmacology—drug disposition, action, and therapy in infants and children. *N Engl J Med*. 2003;349(12):1157-1167. doi:10.1056/NEJMra035092
2. Leeder JS, Meibohm B. Challenges and opportunities for increasing the Knowledge Base related to drug biotransformation and pharmacokinetics during growth and development. *Drug Metab Dispos*. 2016;44(7):916-923. doi:10.1124/dmd.116.071159
3. Brouwer K, Aleksunes L, Brandys B, et al. Human ontogeny of drug transporters: review and recommendations of the pediatric transporter working group. *Clin Pharmacol Therap*. 2015;98(3):266-287. doi:10.1002/cpt.176
4. Cheung KWK, van Groen BD, Spaans E, et al. A comprehensive analysis of ontogeny of renal drug transporters: mRNA analyses, quantitative proteomics, and localization. *Clin Pharmacol Therap*. 2019;106(5):1083-1092. doi:10.1002/cpt.1516
5. Ivanyuk A, Livio F, Biollaz J, Buclin T. Renal drug transporters and drug interactions. *Clin Pharmacokinet*. 2017;56(8):825-892. doi:10.1007/s40262-017-0506-8
6. Morrissey KM, Stocker SL, Wittwer MB, Xu L, Giacomini KM. Renal transporters in drug development. *Annu Rev Pharmacol*

Toxicol. 2013;53(1):503-529. doi:10.1146/annurev-pharmtox-011112-140317
7. Miki Y, Suzuki T, Tazawa C, Blumberg B, Sasano H. Steroid and xenobiotic receptor (SXR), cytochrome P450 3A4 and multidrug resistance gene 1 in human adult and fetal tissues. *Mol Cell Endocrinol*. 2005;231(1):75-85. doi:10.1016/j.mce.2004.12.005
8. Cristea S, Krekels EHJ, Rostami-Hodjegan A, Allegaert K, Knibbe CAJ. The influence of drug properties and ontogeny of transporters on pediatric renal clearance through glomerular filtration and active secretion: a simulation-based study. *AAPS J*. 2020;22(4):87. doi:10.1208/s12248-020-00468-7
9. Edginton AN, Schmitt W, Voith B, Willmann S. A mechanistic approach for the scaling of clearance in children. *Clin Pharmacokinet*. 2006;45(7):683-704. doi:10.2165/00003088-200645070-00004
10. Huang W, Isoherranen N. Development of a dynamic physiologically based mechanistic kidney model to predict renal clearance. *CPT Pharm Syst Pharmacol*. 2018;7(9):593-602. doi:10.1002/psp4.12321
11. Cheung KWK, van Groen BD, Burckart GJ, Zhang L, de Wildt SN, Huang S-M. Incorporating ontogeny in physiologically based pharmacokinetic modeling to improve pediatric drug development: what we know about developmental changes in membrane transporters. *J Clin Pharmacol*. 2019;59(Suppl 1):S56-S69. doi:10.1002/jcph.1489
12. Cristea S, Krekels EHJ, Allegaert K, et al. Estimation of ontogeny functions for renal transporters using a combined population pharmacokinetic and physiology-based pharmacokinetic approach: application to OAT1,3. *AAPS J*. 2021;23(3):65. doi:10.1208/s12248-021-00595-9
13. Ganguly S, Edginton AN, Gerhart JG, et al. Physiologically based pharmacokinetic modeling of meropenem in preterm and term infants. *Clin Pharmacokinet*. 2021;60(12):1591-1604. doi:10.1007/s40262-021-01046-6
14. Ince I, Dallmann A, Frechen S, et al. Predictive performance of physiology-based pharmacokinetic dose estimates for pediatric trials: evaluation with 10 Bayer small-molecule compounds in children. *J Clin Pharmacol*. 2021;61(S1):S70-S82. doi:10.1002/jcph.1869
15. Tod M, Jullien V, Pons G. Facilitation of drug evaluation in children by population methods and modelling. *Clin Pharmacokinet*. 2008;47(4):231-243. doi:10.2165/00003088-200847040-00002
16. Koch AL. The logarithm in biology 1. Mechanisms generating the log-Normal distribution exactly. *J Theor Biol*. 1966;12(2):276-290. doi:10.1016/0022-5193(66)90119-6
17. Lasdon LS, Waren AD, Jain A, Ratner M. Design and testing of a generalized reduced gradient code for nonlinear programming. *ACM Trans Math Softw*. 1978;4(1):34-50. doi:10.1145/355769.355773
18. Edginton AN, Schmitt W, Willmann S. Development and evaluation of a generic physiologically based pharmacokinetic model for children. *Clin Pharmacokinet*. 2006;45(10):1013-1034. doi:10.2165/00003088-200645100-00005
19. Kuepfer L, Niederalt C, Wendl T, et al. Applied concepts in PBPK modeling: how to build a PBPK/PD model. *CPT Pharmacometrics Syst Pharmacol*. 2016;5(10):516-531. doi:10.1002/psp4.12134
20. Watt KM, Cohen-Wolkowiez M, Barrett JS, et al. Physiologically based pharmacokinetic approach to determine dosing on extracorporeal life support: fluconazole in children on ECMO. *CPT: Pharm Syst Pharmacol*. 2018;7(10):629-637. doi:10.1002/psp4.12338
21. Britz H, Hanke N, Taub ME, et al. Physiologically based pharmacokinetic models of probenecid and furosemide to predict transporter mediated drug-drug interactions. *Pharm Res*. 2020;37(12):250. doi:10.1007/s11095-020-02964-z
22. Dubinsky S, Malik P, Hajducek DM, Edginton A. Determining the effects of chronic kidney disease on organic anion Transporter1/3 activity through physiologically based pharmacokinetic modeling. *Clin Pharmacokinet*. 2022;61:997-1012. doi:10.1007/s40262-022-01121-6
23. Miranda PD, Good SS, Krasny HC, Connor JD, Laskin OL, Lietman PS. Metabolic fate of radioactive acyclovir in humans. *Am J Med*. 1982;73(Part 1):215-220. doi:10.1016/0002-9343(82)90094-8
24. Jaehde U, Sörgel F, Reiter A, Sigl G, Naber KG, Schunack W. Effect of probenecid on the distribution and elimination of ciprofloxacin in humans. *Clin Pharmacol Therap*. 1995;58(5):532-541. doi:10.1016/0009-9236(95)90173-6
25. Hiroshi U, Ikumi T, Hikaru Y, et al. Faropenem transport across the renal epithelial luminal membrane via inorganic phosphate transporter Npt1. *Antimicrob Agents Chemother*. 2000;44(3):574-577. doi:10.1128/AAC.44.3.574-577.2000
26. Nishimura M, Naito S. Tissue-specific mRNA expression profiles of human phase I metabolizing enzymes except for cytochrome P450 and phase II metabolizing enzymes. *Drug Metab Pharmacokinet*. 2006;21(5):357-374. doi:10.2133/dmpk.21.357
27. Schmitt W. General approach for the calculation of tissue to plasma partition coefficients. *Toxicol In Vitro*. 2008;22(2):457-467. doi:10.1016/j.tiv.2007.09.010
28. Margaillan G, Rouleau M, Fallon JK, et al. Quantitative profiling of human renal UDP-glucuronosyltransferases and glucuronidation activity: a comparison of Normal and tumoral kidney tissues. *Drug Metab Dispos*. 2015;43(4):611-619. doi:10.1124/dmd.114.062877
29. Momper JD, Tsunoda SM, Ma JD. Evaluation of proposed in vivo probe substrates and inhibitors for phenotyping transporter activity in humans. *J Clin Pharmacol*. 2016;56(S7):S82-S98. doi:10.1002/jcph.736
30. Huang W, Isoherranen N. Novel mechanistic PBPK model to predict renal clearance in varying stages of CKD by incorporating tubular adaptation and dynamic passive reabsorption. *CPT Pharmacometrics Syst Pharmacol*. 2020;9(10):571-583. doi:10.1002/psp4.12553
31. Jones H, Rowland-Yeo K. Basic concepts in physiologically based pharmacokinetic modeling in drug discovery and development. *CPT Pharm Syst Pharmacol*. 2013;2(8):63. doi:10.1038/psp.2013.41
32. Maharaj AR, Edginton AN. Physiologically based pharmacokinetic modeling and simulation in pediatric drug development. *CPT Pharm Syst Pharmacol*. 2014;3(11):148. doi:10.1038/psp.2014.45
33. Abdalla S, Briand C, Oualha M, et al. Population pharmacokinetics of intravenous and Oral acyclovir and Oral valacyclovir in pediatric population to optimize dosing regimens. *Antimicrob Agents Chemother*. 2020;64(12):e01426. doi:10.1128/AAC.01426-20
34. Ohta K, Imamura Y, Okudaira N, Atsumi R, Inoue K, Yuasa H. Functional characterization of multidrug and toxin extrusion protein 1 as a facilitative transporter for fluoroquinolones.

J Pharmacol Exp Ther. 2009;328(2):628-634. doi:10.1124/jpet.108.142257
35. Meyer zu Schwabedissen HE, Verstuyft C, Kroemer HK, Becquemont L, Kim RB. Human multidrug and toxin extrusion 1 (MATE1/SLC47A1) transporter: functional characterization, interaction with OCT2 (SLC22A2), and single nucleotide polymorphisms. *Am J Phys-Renal Phys Ther*. 2010;298(4):F997-F1005. doi:10.1152/ajprenal.00431.2009
36. Park MS, Okochi H, Benet LZ. Is ciprofloxacin a substrate of P-glycoprotein? *Archives Drug Inform*. 2011;4(1):1-9. doi:10.1111/j.1753-5174.2010.00032.x
37. Hernández-Lozano I, Wanek T, Sauberer M, et al. Influence of ABC transporters on the excretion of ciprofloxacin assessed with PET imaging in mice. *Eur J Pharm Sci*. 2021;163:105854. doi:10.1016/j.ejps.2021.105854
38. Lipman J, Gous A, Mathivha L, et al. Ciprofloxacin pharmacokinetic profiles in Paediatric sepsis: how much ciprofloxacin is enough? *Intensive Care Med*. 2002;28(4):493-500. doi:10.1007/s00134-002-1212-y
39. Zhao W, Hill H, Le Guellec C, et al. Population pharmacokinetics of ciprofloxacin in neonates and young infants less than three months of age. *Antimicrob Agents Chemother*. 2014;58(11):6572-6580. doi:10.1128/AAC.03568-14
40. Bakos É, Evers R, Sinkó E, Váradi A, Borst P, Sarkadi B. Interactions of the human multidrug resistance proteins MRP1 and MRP2 with organic anions. *Mol Pharmacol*. 2000;57(4):760-768. doi:10.1124/mol.57.4.760
41. Al-Mohizea AM. Influence of intestinal efflux pumps on the absorption and transport of furosemide. *Saudi Pharm J*. 2010;18(2):97-101. doi:10.1016/j.jsps.2010.02.005
42. Chapa R, Li CY, Basit A, et al. Contribution of uptake and efflux transporters to Oral pharmacokinetics of furosemide. *ACS Omega*. 2020;5(51):32939-32950. doi:10.1021/acsomega.0c03930
43. Peterson RG, Simmons MA, Rumack BH, Levine RL, Brooks JG. Pharmacology of furosemide in the premature newborn infant. *J Pediatr*. 1980;97(1):139-143. doi:10.1016/S0022-3476(80)80154-5
44. Tuck S, Morselli P, Broquaire M, Vert P. Plasma and urinary kinetics of furosemide in newborn infants. *J Pediatr*. 1983;103(3):481-485. doi:10.1016/S0022-3476(83)80433-8
45. Shibayama T, Sugiyama D, Kamiyama E, Tokui T, Hirota T, Ikeda T. Characterization of CS-023 (RO4908463), a novel parenteral carbapenem antibiotic, and meropenem as substrates of human renal transporters. *Drug Metab Pharmacokinet*. 2007;22(1):41-47. doi:10.2133/dmpk.22.41
46. Dong J, Liu Y, Li L, Ding Y, Qian J, Jiao Z. Interactions between meropenem and renal drug transporters. *Curr Drug Metab*. 2022;23(5):423-431. doi:10.2174/1389200223666220428081109
47. van den Anker JN, Pokorna P, Kinzig-Schippers M, et al. Meropenem pharmacokinetics in the newborn. *Antimicrob Agents Chemother*. 2009;53(9):3871-3879. doi:10.1128/AAC.00351-09
48. Blumer JL, Reed MD, Kearns GL, et al. Sequential, single-dose pharmacokinetic evaluation of meropenem in hospitalized infants and children. *Antimicrob Agents Chemother*. 1995;39(8):1721-1725. doi:10.1128/AAC.39.8.1721
49. Gather U, Kale BK. Maximum likelihood estimation in the presence of Outiliers. *Commun Stat – Theory Meth*. 1988;17(11):3767-3784. doi:10.1080/03610928808829834
50. Hayton WL. Maturation and growth of renal function: dosing renally cleared drugs in children. *AAPS PharmSci*. 2000;2(1):22-28. doi:10.1208/ps020103
51. Hines RN. Developmental expression of drug metabolizing enzymes: impact on disposition in neonates and young children. *Int J Pharm*. 2013;452(1):3-7. doi:10.1016/j.ijpharm.2012.05.079
52. Prasad B, Johnson K, Billington S, et al. Abundance of drug transporters in the human kidney cortex as quantified by quantitative targeted proteomics. *Drug Metab Dispos*. 2016;44(12):1920-1924. doi:10.1124/dmd.116.072066
53. Basit A, Radi Z, Vaidya VS, Karasu M, Prasad B. Kidney cortical transporter expression across species using quantitative proteomics. *Drug Metab Dispos*. 2019;47(8):802-808. doi:10.1124/dmd.119.086579
54. Hagos Y, Wolff NA. Assessment of the role of renal organic anion transporters in drug-induced nephrotoxicity. *Toxins*. 2010;2(8):2055-2082. doi:10.3390/toxins2082055
55. Radi ZA. Kidney transporters and drug-induced injury in drug development. *Toxicol Pathol*. 2020;48(6):721-724. doi:10.1177/0192623320937012

SUPPORTING INFORMATION

Additional supporting information can be found online in the Supporting Information section at the end of this article.

How to cite this article: Hunt JP, Dubinsky S, McKnite AM, et al. Maximum likelihood estimation of renal transporter ontogeny profiles for pediatric PBPK modeling. *CPT Pharmacometrics Syst Pharmacol*. 2024;00:1-13. doi:10.1002/psp4.13102